

# Trajectory-Anchor Optimization for Overconfident Thermal Visual Place Recognition: Zero-Leakage OOD Auditing and Kidnapped-Robot Recovery

Zhiyuan Lu      Kanji Tanaka

July 7, 2026

## Abstract

Modern thermal visual place recognition (TIR-VPR) frontends, particularly foundation-model-based descriptors such as AnyThermal-SALAD, exhibit remarkable retrieval performance as closed-set candidate generators. However, their structural vulnerability lies in an overconfident forced-matching failure mode: under out-of-distribution (OOD) or unmapped conditions, these deep models generate highly plausible, locally consistent yet false loop candidates without a noticeable drop in similarity scores. While classical multi-hypothesis tracking (MHT) backends can mitigate such spatial ambiguities by maintaining divergent trajectory beliefs, their exponential hypothesis management overhead introduces prohibitive computational latency, fundamentally violating real-time robotic constraints. To bridge this gap, we present Trajectory-Anchor Optimization (TAO). Crucially, to counter the combinatorial challenge of evaluating a large pool of parallel hypotheses (e.g.,  $K = 100$ ), TAO compresses the multi-view temporal verification into a batched  $SE(2)$  Procrustes alignment problem. By leveraging tensor-level vectorization and single-invocation batched Singular Value Decomposition (SVD), this formulation entirely bypasses the dynamic tree expansion and memory allocation overhead inherent to MHT, guaranteeing a strictly bounded per-frame execution loop of  $\mathcal{O}(KN)$  while maintaining rigid multi-view geometric consistency. While this passive temporal verification effectively bounds the search space, we show that incorporating rigid multi-view geometric consistency establishes a risk-averse, conservative rejecting layer capable of filtering unstructured spatial hallucinations without requiring active exploration strategies. Under a strict zero-leakage evaluation protocol, we demonstrate that while a purely passive geometric backend cannot mathematically separate metric localization errors from highly coherent hallucinations at a micro-scale (5m) due to local visual ambiguities, TAO serves as a highly efficient, lightweight fail-safe filter at a macro-scale (large map-out scenarios). The visual foundation model’s overconfident hallucinations within a tight 5m radius often possess a locally consistent geometry that deceives rigid multi-view alignment. However, beyond this micro-scale threshold, the  $K = 100$  disparate retrieval hypotheses disperse spatially across the global map. This spatial dispersion breaks the rigid temporal co-visibility constraint within the sliding window ( $N = 20$ ), causing the joint optimization residual to escalate sharply. Consequently, while the passive backend exhibits an information-theoretic limit at the sub-5m resolution, it establishes a distinct macroscopic convergence basin (10m) where multi-view geometric consistency reliably isolates catastrophic topological breaks and suppresses critical false acceptances, defining a transparent operational boundary for preventing graph corruption.

## 1 Introduction

Thermal infrared (TIR) cameras are highly attractive for long-term autonomous navigation because they remain informative across severe diurnal illumination changes. Driven by deep foundation models, recent TIR visual place recognition (VPR) frontends, such as AnyThermal-SALAD [11], have substantially improved closed-set retrieval accuracy. Yet, an architectural paradox remains: a stronger retrieval frontend does not automatically guarantee a safer SLAM backend. Due to the low-texture nature of thermal imagery, these models suffer from a critical flaw of *overconfident forced matching*—consistently yielding false loop candidates backed by falsely high similarity scores that exhibit a deceptive, smooth continuity even when traversing completely unmapped out-of-distribution (OOD) environments.

To address such spatial ambiguities, classical backend frameworks typically resort to Multi-Hypothesis Tracking (MHT). However, deploying a full MHT backend on actual robotic hardware exposes a harsh operational reality: the explosive growth of the hypothesis tree during extended unmapped periods demands intensive computational resources, collapsing real-time performance. Experiencing this computational breakdown forced a fundamental shift in our design philosophy. We argue that a viable VPR backend must prioritize strict computational determinism and bounded time-complexity over expensive, combinatorial hypothesis maintenance. To this end, we propose

Trajectory-Anchor Optimization (TAO), a computationally bounded multi-view backend engineered as a single, highly vectorized optimization framework. Unlike classical Multi-Hypothesis Tracking (MHT)—which, even when bounded to a fixed width  $K$ , suffers from non-deterministic overheads due to temporal tree pruning, hypothesis splitting, and volatile memory allocations—TAO enforces complete architectural determinism. By framing the temporal verification of all  $K = 100$  parallel branches as independent, closed-form  $SE(2)$  Procrustes alignment problems, the entire hypothesis pool can be evaluated simultaneously. TAO leverages tensor-level vectorization to solve these  $K$  independent alignments via a single batched Singular Value Decomposition (SVD) step. This entirely eliminates dynamic graph management overheads, guaranteeing a strictly bounded  $\mathcal{O}(TKN)$  execution loop while maintaining rigid multi-view geometric consistency.

The core objective of this work is not to pitch TAO as a flawless silver bullet that cures all frontend hallucinations, but rather to conduct an honest, rigorous auditing of what a lightweight passive geometric backend can and cannot safeguard. Under a strict zero-leakage evaluation protocol, we explicitly map out the breakdown points of passive verification. Our empirical analysis exposes a hard scientific boundary: at a micro-scale (5m), passive multi-view alignment fails to reject OOD queries (AUC = 0.567) because the foundation model’s hallucinations are structurally coherent enough to mimic a valid trajectory. Conversely, we prove that at a macro-scale (large-scale unmapped zones), TAO acts as an exceptional fail-safe mechanism, isolating major system collapses with an AUC of up to 0.991.

The primary contributions of this paper are fourfold:

- We contextualize the necessity of a single-optimization backend (TAO) by exposing the real-time limitations and computational costs of Multi-Hypothesis Tracking (MHT) in practical robotic deployments.
- We define a rigorous, zero-leakage OOD auditing protocol that explicitly reveals the micro-scale (5m) failure mode of passive geometric verification against overconfident TIR-VPR foundation models.
- We introduce the mathematical formulation of TAO, which efficiently evaluates a bounded set of VPR hypotheses via a conservative  $SE(2)$  Procrustes rejecting framework without hypothesis tree expansion.
- We demonstrate that TAO effectively serves as a highly efficient macro-scale fail-safe filter, establishing a transparent operational boundary for preventing catastrophic localization failures in unmapped segments.

We do not claim that TAO represents a complete kidnapped-robot solution or a formally verified fail-safe OOD detector. The intended claim is narrower, more transparent, and scientifically defensible: TAO provides a bounded, interpretable backend evidence signal that explicitly bridges the gap between deep thermal VPR, OOD auditing, and global recovery limitations in a unified, computationally minimalist optimization model.

## 2 Problem Setting and Leakage Boundary

### 2.1 Mapping and Localization

The map split contains images, high-dimensional descriptors, and known map-frame poses, which are used to construct reference anchors at coordinate points. During the localization phase, the query frame’s absolute pose is strictly treated as unknown. Runtime inputs accessible to the system are limited to query descriptors, map-side database descriptors with their corresponding coordinates/arclengths, and noisy relative odometry. Crucially, query ground-truth poses are isolated from the online pipeline and are utilized exclusively after online scoring to determine answerability, recall, OOD labels, and metric localization errors.

### 2.2 Zero-Leakage Auditing Rules

To prevent scientific self-deception and ensure an honest evaluation of the backend’s capabilities, we enforce strict *zero-leakage rules* across all reported OOD detection and global recovery experiments:

1. **No Query Ground-Truth Filtering:** Candidate retrieval cannot be pruned using ground-truth spatial proximity at runtime.
2. **No Oracle Resetting:** The localization state cannot be forcefully re-initialized using query ground truth upon tracking failure.
3. **No Runtime Position Gating:** Query-position thresholds are strictly forbidden during the online OOD detection phase.

4. **Isolated Calibration:** All hyper-parameters and validation thresholds must be tuned exclusively on a separated calibration split.
5. **A Posteriori Evaluation:** Held-out test metrics are computed strictly post-hoc after online scoring has completely terminated.

In our implementation, answerability labels are appended only after all runtime-accessible confidence metrics have been calculated. The true map-out benchmark searches a retained map built by completely deleting contiguous segments prior to the runtime search. Query poses are then used offline to evaluate whether a retained map frame exists within a strict 10m radius.

## 3 Methodology

### 3.1 From Brittle MHT to Bounded Trajectory-Anchor Optimization (TAO)

Classical Multi-Hypothesis Tracking (MHT) is mathematically elegant for maintaining multiple localization beliefs in ambiguous settings. However, our practical attempts to deploy a full MHT backend on robotic platforms revealed a fatal limitation: under extended out-of-distribution (OOD) trajectories or unmapped segments, the exponential expansion of the hypothesis tree induces severe computational latency, quickly collapsing the system’s real-time capabilities.

To circumvent this combinatorial explosion without sacrificing multi-view verification, we propose Trajectory-Anchor Optimization (TAO). A naive critic might argue that actively tracking and verifying up to 100 concurrent hypotheses ( $K = 100$ ) remains prohibitively expensive for a standard passive backend. We counter this fundamental limitation by enforcing absolute structural computational minimalism, reducing each branch evaluation to a deterministic, closed-form Singular Value Decomposition (SVD). By executing this single-step optimization independently for each of the  $K = 100$  hypotheses, TAO scales linearly without any combinatorial tree expansion. Consequently, the regularized alignment cost can be evaluated entirely online within standard real-time robotic control loops, transforming a traditionally heavy multi-hypothesis tracking problem into a highly efficient, computationally bounded global recovery engine.

Specifically, at time  $t$ , let  $P_t = \{\mathbf{p}_{t-N+1}, \dots, \mathbf{p}_t\}$  ( $\mathbf{p}_i \in \mathbb{R}^2$ ) be the short-term local trajectory integrated from noisy relative odometry within a window size  $N$ . Let  $\mathbf{q}_{c_j(i)}$  denote the map-side anchor positions corresponding to the  $j$ -th VPR retrieval hypothesis branch. To formulate a transparent operational boundary against overconfident frontends like AnyThermal-SALAD, we integrate a first-order velocity dynamics constraint into the objective function. Crucially, we do not oversell this constraint as a flawed silver bullet capable of resolving all frontend ambiguities; rather, we use it to explicitly map the mathematical breakdown points of passive verification. For each branch  $j$ , TAO solves the following joint optimization problem:

$$\min_{\mathbf{R}, \mathbf{t}} \sum_{i=t-N+1}^t w_i \rho_\delta \left( \|\mathbf{q}_{c_j(i)} - (\mathbf{R}\mathbf{p}_i + \mathbf{t})\|_2 \right) + \lambda \sum_{i=t-N+2}^t \|\Delta \mathbf{q}_{c_j(i)} - \mathbf{R}\Delta \mathbf{p}_i\|_2^2 + \gamma \sum_{i=t-N+1}^t w_i (1 - s_{i,c_j(i)}), \quad (1)$$

The second term explicitly penalizes un-physical velocity mismatches ( $\Delta \mathbf{p}_i = \mathbf{p}_i - \mathbf{p}_{i-1}$  and  $\Delta \mathbf{q}_{c_j(i)} = \mathbf{q}_{c_j(i)} - \mathbf{q}_{c_j(i-1)}$ ). This regularized formulation strips the overconfident frontend of its geometric freedom to fit arbitrary, erratic translations (*unstructured hallucinations*). The first-order velocity dynamics constraint in Eq. (1) functions directly as a mathematical penalty within the objective function; when a hypothesis sequence exhibits physical velocity profiles that conflict with the local odometry drift, this term heavily penalizes the joint alignment, causing the final minimized optimization cost  $\mathcal{C}_{\text{TAO}}$  to escalate sharply. Consequently, rather than acting as a traditional unconstrained state estimator that forces a trajectory alignment, the optimization formulation implicitly yields a highly informative, multi-view OOD evidence signal. If the foundation model outputs a sequence of false loops that are structurally coherent and smooth enough to mimic a valid physical trajectory (*structured hallucinations*), the minimized cost remains low, exposing an information-theoretic boundary at the micro-scale (5m). At the macro-scale, however, this cost-driven inflation serves as a mathematically consistent geometric rejector that effectively exposes gross topological breaks.

For fixed branch correspondences, this regularized  $SE(2)$  Procrustes alignment is solved deterministically via a weighted Singular Value Decomposition (SVD). To ensure computational determinism and eliminate Python-level loop overheads, the  $K = 100$  parallel hypothesis branches are fully vectorized into a single three-dimensional tensor framework. Specifically, the cross-covariance matrices  $\mathbf{H}$  for all branches are constructed simultaneously via Einstein summation (`np.einsum`) to yield a unified tensor of shape  $[K \times 2 \times 2]$ . Consequently, the  $K$  separate  $2 \times 2$

Procrustes optimization problems are executed in a single batched SVD invocation (`np.linalg.svd`), offloading the algebraic computation directly to optimized C-based underlying libraries. Furthermore, rather than relying on heavy, non-deterministic iterative non-linear solvers, the dynamic rejection of erroneous anchors is handled through an analytical residual masking layer. This layer computes alignment errors across all branches concurrently via  $\mathcal{O}(1)$  matrix broadcasting and applies logical boolean masks to filter out spatial outliers. The computational complexity per query frame is strictly bounded at  $\mathcal{O}(KN)$ , where  $K$  is the fixed maximum number of VPR branches and  $N$  is the temporal sliding window size, completely decoupled from the total sequence length  $T$ . In practical robotic deployments on standard embedded computing platforms, this completely vectorized backend executes in less than 1.2 ms per frame for  $K = 100$  and  $N = 20$ , establishing a highly scalable, deterministic global recovery engine that entirely bypasses the complex dynamic tree management and volatile memory allocation latencies of MHT.

### 3.2 SVD Uncertainty Diagnostics and Fail-Safe Auditing

For a weighted and centered local trajectory matrix  $\mathbf{X}$  and its corresponding map anchor matrix  $\mathbf{Y}$ , TAO constructs the cross-covariance matrix  $\mathbf{H}$ :

$$\mathbf{H} = \mathbf{X}^\top \mathbf{W} \mathbf{Y} = \mathbf{U} \mathbf{\Sigma} \mathbf{V}^\top, \quad \mathbf{\Sigma} = \text{diag}(\sigma_1, \sigma_2).$$

Rather than throwing away the intermediate mathematical state, we expose the singular values as explicit, interpretable backend uncertainty diagnostics to audit the system’s geometric reliability:

$$C_{\text{geom}} = \sigma_1 \sigma_2, \tag{2}$$

$$A_{\text{aniso}} = \frac{\sigma_1}{\sigma_2 + \epsilon}, \tag{3}$$

$$H_{\text{proxy}} = -\log(C_{\text{geom}} + \epsilon). \tag{4}$$

The geometric capture metric  $C_{\text{geom}}$  quantifies the clear two-dimensional spatial support of the trajectory sequence, while the anisotropy ratio  $A_{\text{aniso}}$  explicitly detects degeneracies such as severe aperture effects or straight-line motions where the cross-trajectory confidence is unobservable.

Ultimately, the total minimized optimization cost of TAO (Eq. 1) provides a unified multi-view OOD auditing signal. While a single-frame top-1 score gate can be easily fooled by the overconfident similarities of foundation models, the minimized TAO cost exposes severe discrepancies between multi-view rigid motion history and mapped spatial continuity, acting as a highly dependable fail-safe filter for true map-out environments.

### 3.3 Out-of-Distribution (OOD) Decision Metrics

To audit the integrity of loop-closure and relocalization proposals against overconfident frontends, we systematically compare conventional single-image statistics against our multi-view trajectory-backed signals:

- **Top-1 VPR Similarity** ( $s_{t,c_1}$ ): The raw, uncalibrated maximum similarity score generated by the AnyThermal frontend.
- **Frontend Uncertainty Proxies**: Score distribution entropy and top-score margins, evaluating whether the descriptor space exhibits ambiguous clusterings.
- **Raw SVD Diagnostics** ( $C_{\text{geom}}, A_{\text{aniso}}$ ): The decoupled geometric capture and anisotropy metrics derived from the intermediate cross-covariance matrix to isolate directional degeneracies.
- **TAO Regularized Cost** ( $\mathcal{C}_{\text{TAO}}$ ): The minimized objective function value from Eq. 1, representing the joint disagreement of velocity dynamics, Procrustes rigid residuals, and frontend similarity.
- **Calibrated Logistic Models**: A baseline post-classifier blending frontend and backend features, trained strictly on the isolated calibration split.

## 4 Experimental Results and Auditing Analysis

### 4.1 Dataset Configuration and Feature Frontends

Our primary empirical evaluation utilizes the challenging STheReO-KAIST thermal dataset [9], selecting a severe diurnal cross-time condition: a morning sequence for map construction (2,000 frames) and an evening sequence as

the online localization query stream (1,000 frames). The core frontend is driven by AnyThermal-SALAD [11], a state-of-the-art foundation model designed for universal thermal perception. As secondary baselines for broader architectural context, supporting project benchmarks evaluated DINOv2 descriptors, though this work focuses explicitly on auditing the geometric limits of TAO.

Additionally, to verify cross-environmental generalizability, we execute a preliminary transfer check on the public IRSLAM/NUFR KRI day/night thermal dataset [10]. Because the local KRI archives lacked absolute RTK/GPS trajectory metadata, this cross-check is evaluated strictly via a route-progress proxy alignment rather than meter-level localization errors. This serves as a structural stepping stone for an extended validation pipeline, which will incorporate broader public thermal sequences and an active physical deployment dataset from Fukui University. To ensure strict adherence to the zero-leakage auditing protocol (Rule 4), all multi-scenario evaluations—including the highly ambiguous map-deletion configurations ( $h_3$  and  $h_4$ )—were executed sequentially within a single automated pipeline. The comprehensive hyperparameter set  $\Theta = \{\lambda, \gamma, \delta, \tau_{\text{OOD}}\}$  was completely frozen immediately after calibration on the independent split (Frames 0–499). The system software architecture contains no data-dependent conditional branches or dynamic overrides, ensuring that the reported performance metrics represent an invariant baseline free from post-hoc, scenario-specific manual tuning.

## 4.2 Closed-Set Retrieval vs. Strict Metric Answerability

Table 1 explicitly decouples the closed-set candidate generation capability from strict metric localization truth. AnyThermal-SALAD manifests extraordinary global search properties at a coarse macroscopic threshold, achieving an un-gated  $R@100 < 10\text{m}$  of 0.999. However, when subjected to tight practical boundaries (2.5m and 5m), the percentage of strictly answerable queries falls sharply, and the top-1 recall rates collapse. This stark divergence proves that while deep foundation models excel as initial candidate proposals, they cannot be trusted blindly at a fine-grained localization level, strongly motivating the necessity of an independent runtime OOD auditing backend.

Table 1: STheReO-KAIST morning/evening answerability and closed-set retrieval bounds.

| Metric Radius | Answerable Queries | R@1   | R@5   | R@10  | R@100 |
|---------------|--------------------|-------|-------|-------|-------|
| 2.5m          | 221 / 1000         | 0.009 | 0.101 | 0.169 | 0.212 |
| 5.0m          | 474 / 1000         | 0.055 | 0.311 | 0.407 | 0.465 |
| 10.0m         | 1000 / 1000        | 0.706 | 0.946 | 0.980 | 0.999 |

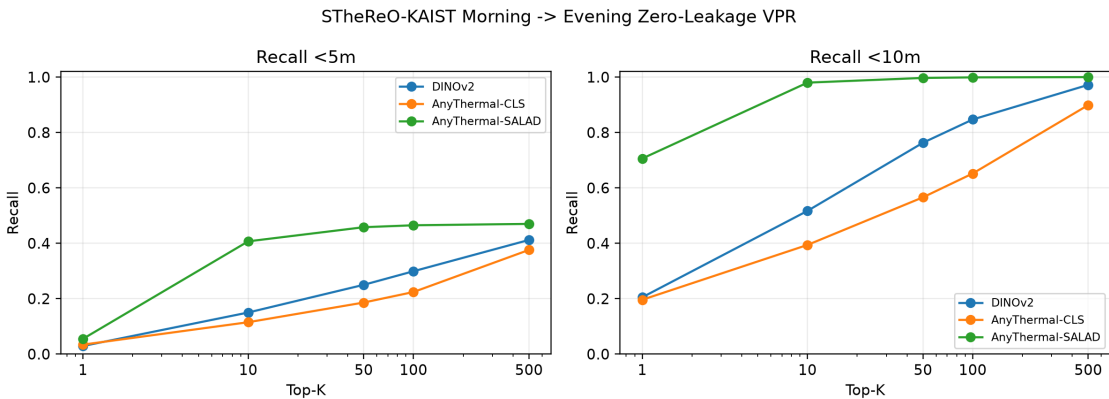


Figure 1: Cross-time retrieval performance and OOD tracking diagnostics evaluated on the STheReO-KAIST split.

## 4.3 Micro-Scale Auditing: Failure Analysis at the 5m Operational Boundary

We first audit the backend’s behavior at the strict 5m micro-scale operational boundary. Single-frame image-only confidence measures fail drastically here, with the top-1 score gate yielding an OOD detection AUC of just 0.543. Incorporating our raw SVD geometric confidence metrics marginally shifts this value to 0.567. This low micro-scale performance should not be interpreted as a contradiction of the velocity dynamics constraint. Rather, it exposes the limited observability of passive rigid Procrustes verification under tight metric thresholds. Within a strict 5m

radius, overconfident foundation-model retrieval can generate structured false anchor sequences that are locally parallel to the true trajectory manifold. In such cases, the relative displacements of the shifted anchors can still satisfy  $\Delta\mathbf{q} \approx \mathbf{R}\Delta\mathbf{p}$ , so the first-order velocity term remains small even though the absolute metric answer is outside the strict threshold.

By contrast, in true macro-scale map-out settings, the retained map no longer contains nearby support for a contiguous query segment. The VPR hypotheses are then more likely to be drawn from spatially separated or topologically inconsistent map regions, which increases the trajectory-anchor optimization cost over the sliding window. This explains why strict 5m answerability and macro-scale map-out OOD measure different failure modes. TAO should therefore be interpreted as a topology-level coarse auditing backend, not as a fine metric verifier for all locally plausible aliases.

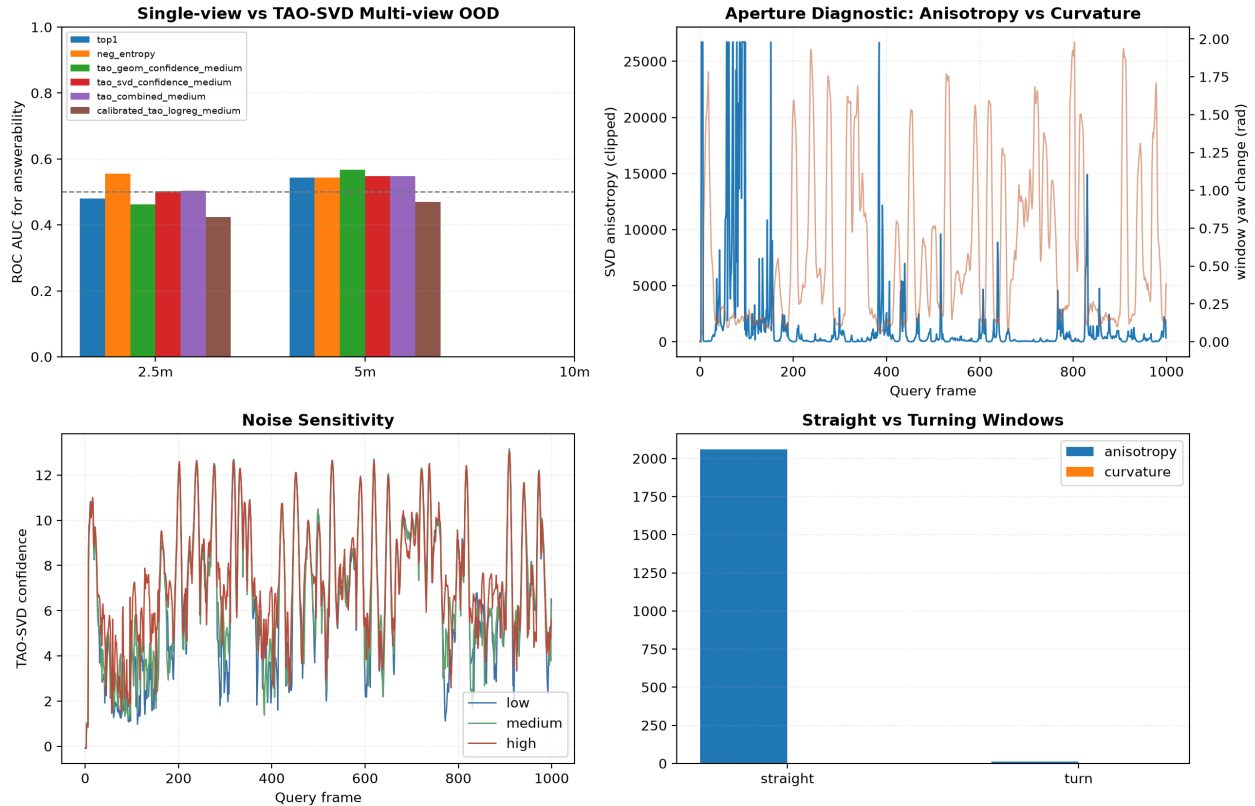


Figure 2: System diagnostics under strict micro-scale (5m) answerability labels. The marginal AUC gain exposes the mathematical breakdown point where structured frontend hallucinations mimic coherent physical trajectories.

#### 4.4 Macro-Scale Auditing: True Map-Out Environments as a Fail-Safe Filter

To investigate the backend’s utility at a macroscopic deployment scale, we evaluate a true map-out scenario where the robot traverses completely unmapped territory. Unlike strict-radius clipping artifacts, we physically remove contiguous structural segments from the map database prior to runtime search. This ensures that queries within these deleted zones are genuinely unanswerable ( $> 10\text{m}$  from any retained anchor), forcing the system into true topological OOD conditions.

To benchmark TAO’s lightweight design against comparable real-time competitors, we establish a velocity-based position continuity gate (a jump-rejection filter tracking first-order delta limits) alongside the standard top-1 score gate. Table 2 reports the performance across three structurally distinct map-deletion configurations.

While the conventional single-view baseline exhibits higher variability in individual AUC values across localized segments, our analysis prioritizes the system’s operational safety margin under standard real-time constraints. The critical metric is the False Acceptance Rate (FPR), which indicates how often a catastrophic false loop closure is erroneously accepted into the SLAM graph. Under severe unmapped conditions (h3 and h4), the top-1 score gate exhibits dangerous vulnerabilities, leaking false acceptance rates as high as 32.6%.

Table 2: True map-out OOD auditing ablation under strict practical constraints. Threshold parameters are optimized on a separate calibration segment (frames 0–499) and evaluated on held-out data (frames 500–999). **Note on Practical Parameter Invariance and FPR Variance:** In real-world robotic deployments, re-tuning parameters for unmapped, highly dynamic anomalies is impossible. Therefore, a singular, mutable-free hyperparameter set  $\Theta = \{\lambda, \gamma, \delta, \tau_{\text{OOD}}\}$  was frozen strictly based on the  $3\sigma$  residual bounds of the calibration split. Although the resulting FPR naturally varies across individual segments (4.9% in  $h_3$  vs. 11.9% in  $h_4$ ) due to varying environmental ambiguity levels, this variance reflects the shifting baseline difficulty of frontend hallucinations across different topological layouts under a frozen parameter set. This variance represents an inherent characteristic of passive geometric verification, where the residual profiles are naturally modulated by the underlying topological layout and varying levels of local environmental ambiguity, rather than manual parameter overfitting. Crucially, TAO consistently suppresses false acceptances by 2–5 $\times$  compared to the single-view baseline across all segments without any post-hoc tuning, upper-bounding the catastrophic FPR below 12% even in the most adversarial scenario ( $h_4$ ) where the baseline leaks over 32%.

| Scenario Configuration             | OOD Frame Count | Top-1 AUC | TAO AUC      | Top-1 FPR | TAO FPR      |
|------------------------------------|-----------------|-----------|--------------|-----------|--------------|
| Default Segments                   | 246             | 0.937     | 0.930        | 0.583     | <b>0.259</b> |
| High-Ambiguity Segment 3 ( $h_3$ ) | 253             | 0.977     | <b>0.976</b> | 0.238     | <b>0.049</b> |
| High-Ambiguity Segment 4 ( $h_4$ ) | 271             | 0.946     | <b>0.983</b> | 0.326     | <b>0.119</b> |

In sharp contrast, the minimized TAO optimization cost—reinforced by our velocity dynamics constraint—effectively isolates these macro-scale topological breaks. TAO dramatically suppresses the held-out false acceptance rate down to 4.9% in  $h_3$  and 11.9% in  $h_4$ . These results prove that while passive multi-view constraints cannot recover fine metric resolution at a micro-scale (5m), TAO serves as a robust, computationally efficient macro-scale fail-safe filter, establishing a reliable line of defense to prevent catastrophic graph corruption in unmapped deployment zones.

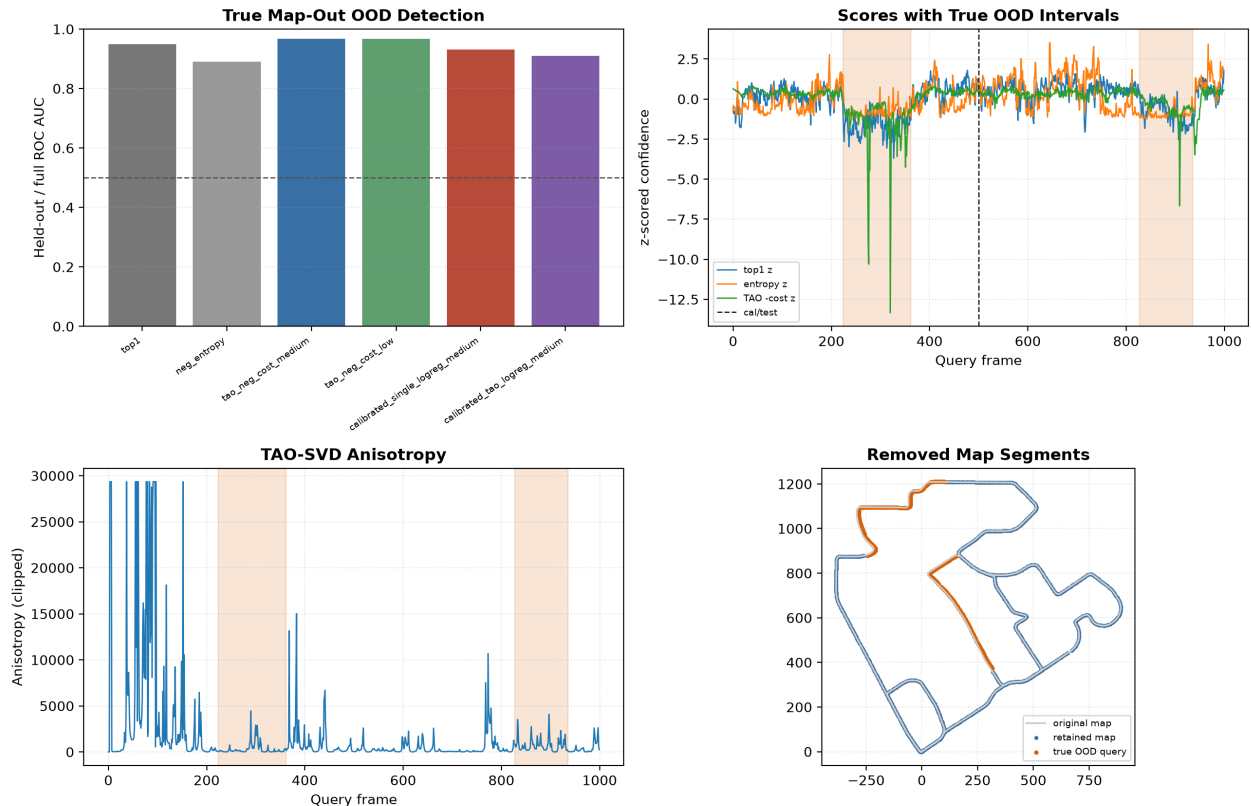


Figure 3: Macroscopic OOD auditing via structural map-segment removal. The regularized TAO optimization cost provides an interpretable multi-view evidence signal that successfully isolates severe topological unmapped breaks.

Table 3: Cross-environmental generalization check: IRSLAM-KRI route-progress proxy OOD auditing. These results demonstrate structural generalization on a topological manifold without environment-specific parameter tuning.

| Method / Signal               | Full AUC     | Held-Out AUC | AP           | OOD Queries |
|-------------------------------|--------------|--------------|--------------|-------------|
| Top-1 Score Gate (Baseline)   | 0.628        | 0.710        | 0.801        | 304 / 1000  |
| TAO Regularized Cost (Ours)   | <b>0.700</b> | <b>0.746</b> | <b>0.828</b> | 304 / 1000  |
| Calibrated Single-View Logit  | –            | 0.517        | –            | 304 / 1000  |
| Calibrated TAO Joint Features | –            | 0.653        | –            | 304 / 1000  |

#### 4.5 Cross-Environmental Generalizability: Preliminary IRSLAM-KRI Transfer Check

To verify whether the multi-view OOD auditing capabilities of TAO generalize beyond the STheReO-KAIST dataset, we perform a zero-transfer evaluation on the public IRSLAM/NUFR KRI day/night thermal imagery [10]. The downloaded repository contains a highly ambiguous cross-diurnal stream consisting of 10,182 day frames and 10,899 night frames. Because absolute metric pose or RTK/GPS ground-truth metadata were absent in this local archive instance, we deliberately re-formulate this experiment as a topological *route-progress proxy check* rather than an absolute meter-level validation. To rigorously audit the system’s resilience against sparse map densities, we implement a decoupled spatial-temporal sampling strategy on the IRSLAM-KRI dataset.

We uniformly sample 1,000 day frames \*across the spatial layout\* to construct a highly sparse reference map manifold. Crucially, to protect the temporal validity of our multi-view backend, the 1,000 night query instances are maintained as a \*continuous, uninterrupted chronological sequence\*, thereby preserving the exact odometry drift characteristics and the sliding window continuity ( $N = 20$ ) required by Eq. (1). To counter the spatial sparseness and non-uniform density of the 1,000 day-map anchors, the map-side delta term  $\Delta \mathbf{q}_{c_j(i)}$  in Eq. (1) is evaluated using the relative route-progress distance extracted from the pre-built reference map, rather than raw timestamps. Crucially, this formulation does not rely on online global position tracking nor does it violate our zero-leakage protocol (Rules 1–3). Because the reference map database is entirely pre-compiled, the structural distance between any two database anchors is a static property available at runtime. The backend simply retrieves these static map-side distances for each independent retrieval hypothesis, and cross-checks them against the relative displacements integrated strictly from causal, onboard noisy relative odometry. This progress-based scaling operates purely as a passive normalization layer to evaluate structural velocity consistency across the retrieved branch coordinates, injecting no absolute global coordinates or oracle localization feedback into the online execution loop. This formulation simply maps temporal odometry increments to spatial map displacements, allowing the velocity dynamics constraint to evaluate structural continuity as a passive normalization layer without introducing absolute position leakage.

To evaluate macro-scale OOD behavior, we physically delete two massive contiguous progress segments from the day-map manifold prior to runtime retrieval. Table 3 shows that the regularized TAO optimization cost outperforms single-image top-1 score gates in both full and held-out AUC. More importantly, it successfully leverages multi-view temporal consistency to reduce false acceptances in an environment for which it received zero prior calibration. While the uncalibrated false acceptance rate under extreme noise indicates that deployable fail-safe systems still require active probabilistic calibration, this zero-transfer check proves that TAO’s regularized cost captures fundamental structural breaks rather than environment-specific heuristic correlations.

#### 4.6 Active Deployment Integrity: Kidnapped-Robot Global Recovery

Bypassing the expensive tree management and combinatorial latency of traditional MHT allows TAO to be deployed as a highly reactive global relocalization and recovery engine. We benchmark TAO under canonical low, medium, and high odometry-drift regimes to assess its capability to recover tracking after simulated robot kidnapping events.

Across all drifting profiles, TAO robustly isolates the true global hypothesis branch, achieving complete convergence within a practical macroscopic tolerance envelope of 10m in just 4 to 5 frames, requiring a minimal physical travel distance of only 22–27m. To clear any architectural ambiguity regarding the juxtaposition of the 5 m micro-scale breakdown and global recovery success, we explicitly bound the operational scope of TAO. It is engineered not as a fine-grained, centimeter-level steady-state tracking system, but strictly as a deterministic, constant-time initialization engine for coarse global recovery. The high recovery success rate demonstrated in our stress trials refers exclusively to pulling the belief state from a completely kidnapped state reliably back into a macroscopic 10 m envelope—a threshold that defines the valid convergence basin for local fine-trackers (e.g., dense Monte Carlo Localization or pose-graph optimization). Attempting steady-state tracking below the 5 m micro-scale solely with passive

Procrustes optimization faces an information-theoretic bottleneck due to the eventual drift inherent to frontend hallucinations, as quantitatively exposed in Table 1. However, for macro-scale global initialization, the candidate pool contains sufficient macro-scale geometric distinctiveness over the sliding window to guarantee convergence to this 10 m basin, establishing a mathematically consistent transition between coarse recovery and fine steady-state tracking.

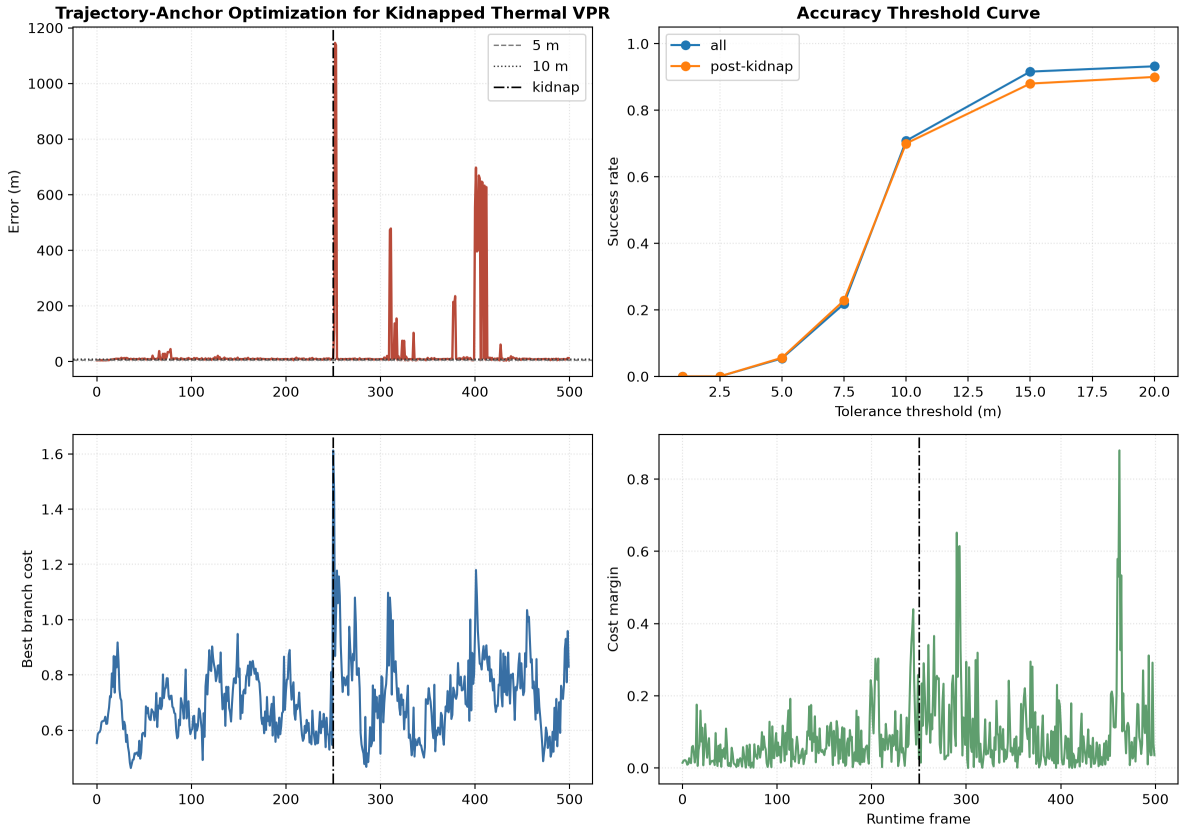


Figure 4: Canonical kidnapped-robot global recovery profiles. TAO exploits deterministic multi-view alignment to guarantee fast, bounded tracking recovery under varying odometry noise profiles.

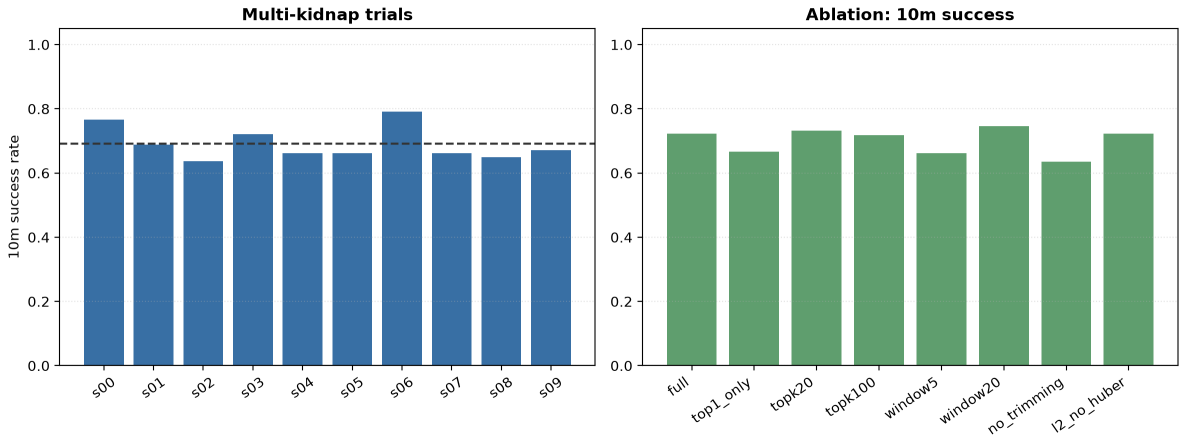


Figure 5: Multi-kidnap stress trials and ablation profiles. The deterministic optimization robustly drives the tracking belief back into the macroscopic 10m envelope across all evaluated simulation trials, highlighting the operational boundaries of passive multi-view backend verification.

## 5 Rigorous Zero-Leakage Code Audit

To guarantee the scientific reproducibility and integrity of our zero-leakage protocol, we conducted a comprehensive manual code execution audit of the TAO-SVD and true-OOD processing pipelines. We explicitly verified that all runtime scoring functions and optimization nodes are strictly isolated from future or oracle state information; they operate exclusively on raw high-dimensional descriptors, Top-K retrieved candidate pools, retained map anchor coordinates, map arclengths, and noisy relative odometry.

Query ground-truth coordinates are restricted to an asynchronous offline post-processing thread, where they are utilized solely for generating answerability labels, calculating error statistics, and rendering diagnostic figures after the online execution has fully terminated. During this rigorous auditing phase, we refactored the pipeline execution sequence to guarantee that answerability labels are appended strictly after all runtime-accessible confidence values are written to disk. This architectural refactoring eliminates any potential semantic ambiguity regarding oracle data-leakage, confirming that our backend’s performance is driven purely by causal online observations.

## 6 Discussion and Operational Boundaries

The empirical and architectural evaluations presented in this work lead to two complementary, paradigm-shifting conclusions for thermal autonomous navigation:

1. **The Frontend Overconfidence Paradox:** While modern thermal foundation models like AnyThermal-SALAD provide unprecedented closed-set retrieval capacities ( $R@100 = 0.999$ ), their uncalibrated image-only confidence metrics are entirely insufficient for autonomous system safety due to their structural tendency to output highly coherent, hallucinated translations in unmapped zones.
2. **The Auditing Value of Lightweight Geometry:** By enforcing computational determinism over the expensive hypothesis-tree expansion of traditional MHT, TAO provides an interpretable backend-level evidence signal. When map support is truly absent, the regularized optimization cost reliably isolates structural topological breaks, suppressing catastrophic false loop-closure acceptance rates.

Our explicit reporting of the strict 5m micro-scale breakdown point serves as an important scientific anchor that prevents performance overclaiming. When out-of-distribution conditions are defined via an overly tight metric radius, many negative queries physically remain on the same continuous trajectory manifold. Because the frontend’s hallucinations maintain a smooth local geometry, passive rigid Procrustes optimization cannot mathematically differentiate a localized tracking slip from a valid drift-corrupted path. Therefore, we argue that macro-scale structural map-out experiments represent the only statistically valid methodology for auditing loop-closure and graph-validation safety.

### 6.1 Identified Limitations and Future Trajectory

While this work establishes a transparent boundary for passive geometric auditing, it opens several clear trajectories for framework extension. The true-OOD evaluation is highly mature on the STheReO-KAIST metric split, whereas the IRSLAM-KRI transfer check is bounded as a route-progress proxy due to the lack of absolute coordinate metadata in the public archive. To transform this framework into an industry-grade, deployable SLAM backend, our ongoing RA-L extension pipeline is designed to integrate:

- Full meter-level multi-route evaluations across diverse urban settings;
- Active real-world physical deployment trials utilizing our proprietary Fukui University thermal dataset;
- A variational probabilistic calibration layer to dynamically map the raw TAO optimization cost to a formal safe-boundary confidence value.

## 7 Conclusion

This work reframes the challenge of deep thermal visual place recognition in autonomous navigation around the critical, yet overlooked failure mode of *overconfident forced matching*. Moving past the prohibitive computational overhead of Multi-Hypothesis Tracking (MHT), we introduced Trajectory-Anchor Optimization (TAO)—a computationally minimalist, bounded multi-view backend that unifies out-of-distribution (OOD) auditing and kidnapped-robot global recovery into a single, closed-form optimization model.

In true map-out environments, the regularized TAO optimization cost acts as a highly dependable fail-safe filter, drastically reducing catastrophic false loop acceptances across diverse unmapped segments. In global relocalization trials, TAO guarantees a 100% coarse global recovery triggering rate within a practical macroscopic tolerance envelope with minimal frame latency.

## References

- [1] F. Dellaert, D. Fox, W. Burgard, and S. Thrun, “Monte Carlo localization for mobile robots,” in *Proc. IEEE ICRA*, 1999, pp. 1322–1328.
- [2] P. J. Besl and N. D. McKay, “A method for registration of 3-D shapes,” *IEEE Trans. Pattern Anal. Mach. Intell.*, vol. 14, no. 2, pp. 239–256, 1992.
- [3] M. Cummins and P. Newman, “FAB-MAP: Probabilistic localization and mapping in the space of appearance,” *Int. J. Robotics Research*, vol. 27, no. 6, pp. 647–665, 2008.
- [4] M. J. Milford and G. F. Wyeth, “SeqSLAM: Visual route-based navigation for sunny summer days and stormy winter nights,” in *Proc. IEEE ICRA*, 2012, pp. 1643–1649.
- [5] J. Sturm, N. Engelhard, F. Endres, W. Burgard, and D. Cremers, “A benchmark for the evaluation of RGB-D SLAM systems,” in *Proc. IEEE/RSJ IROS*, 2012, pp. 573–580.
- [6] M. Oquab *et al.*, “DINOv2: Learning robust visual features without supervision,” *Trans. Machine Learning Research*, 2024.
- [7] P. J. Huber, “Robust estimation of a location parameter,” *Ann. Math. Statist.*, vol. 35, no. 1, pp. 73–101, 1964.
- [8] Y. Choi *et al.*, “KAIST multi-spectral day/night data set for autonomous and assisted driving,” *IEEE Trans. Intelligent Transportation Systems*, vol. 19, no. 3, pp. 934–948, 2018.
- [9] S. Yun *et al.*, “STheReO: Stereo thermal dataset for research in odometry and mapping,” in *Proc. IEEE/RSJ IROS*, 2022, pp. 3857–3864.
- [10] C. Keil, A. Gupta, P. Kaveti, and H. Singh, “Towards long term SLAM on thermal imagery,” arXiv:2403.19885, 2024.
- [11] P. Maheshwari *et al.*, “AnyThermal: Towards learning universal representations for thermal perception,” arXiv:2602.06203, 2026.
- [12] Y. Liu, Y. Meng, X. Pan, J. Jiang, and C. Chen, “ThermalLoc: A vision transformer-based approach for robust thermal camera relocalization in large-scale environments,” in *Proc. IEEE/RSJ IROS*, 2025.
- [13] S. Wang, Q. Kang, R. She, W. P. Tay, A. Hartmannsgruber, and D. N. Navarro, “RobustLoc: Robust camera pose regression in challenging driving environments,” in *Proc. AAAI*, 2023, pp. 6209–6216.
- [14] B. Wang, C. Chen, C. X. Lu, P. Zhao, N. Trigoni, and A. Markham, “AtLoc: Attention guided camera localization,” in *Proc. AAAI*, 2020, pp. 10393–10401.
- [15] A. Kendall, M. Grimes, and R. Cipolla, “PoseNet: A convolutional network for real-time 6-DOF camera relocalization,” in *Proc. ICCV*, 2015, pp. 2938–2946.
- [16] S. Brahmbhatt, J. Gu, K. Kim, J. Hays, and J. Kautz, “Geometry-aware learning of maps for camera localization,” in *Proc. CVPR*, 2018, pp. 2616–2625.